Imaging the *Fermi* γ-ray sky

Marco Selig

IBM Deutschland Research and Development GmbH, Schönaicher Straße 220, D-71032 Böblingen
Max Planck Institut für Astrophysik, Karl-Schwarzschild-Straße 1, D-85748 Garching, Germany
Ludwig-Maximilians-Universität München, Geschwister-Scholl-Platz 1, D-80539 München, Germany
E-mail: mselig@mpa-garching.mpg.de

Valentina Vacca[*]

Max Planck Institut für Astrophysik, Karl-Schwarzschild-Straße 1, D-85748 Garching, Germany
E-mail: vvacca@mpa-garching.mpg.de

Niels Oppermann

Canadian Institute for Theoretical Astrophysics, 60 St. George Street, Toronto, ON M5S 3H8, Canada
E-mail: niels@cita.utoronto.ca

Torsten Enßlin

Max Planck Institut für Astrophysik, Karl-Schwarzschild-Straße 1, D-85748 Garching, Germany
Ludwig-Maximilians-Universität München, Geschwister-Scholl-Platz 1, D-80539 München, Germany
E-mail: ensslin@mpa-garching.mpg.de

We analyze the 6.5 year all-sky data from the *Fermi* Large Area Telescope in the energy range 0.6–307.2 GeV. Raw count maps show a superposition of diffuse and point-like emission structures and are subject to shot noise and instrumental artifacts. Using the Denoising, Deconvolving, and Decomposing Photon Observations D^3PO algorithm, we modeled the observed photon counts as the sum of a diffuse and a point-like photon flux, convolved with the instrumental beam and subject to Poissonian shot noise, without the use of spatial or spectral templates. The D^3PO algorithm performs a Bayesian inference and yields separate estimates for the two flux components. We show that the diffuse γ-ray flux can be described phenomenologically by only two distinct components: a soft component, presumably dominated by hadronic processes, tracing the dense, cold interstellar medium, and a hard component, presumably dominated by leptonic interactions, following the hot and dilute medium and outflows such as the *Fermi* bubbles.

The 34th International Cosmic Ray Conference,
30 July- 6 August, 2015
The Hague, The Netherlands

---

[*]Speaker.

1. Introduction

Since August 2008 the *Fermi* Gamma-ray Space Telescope has observed the γ-ray sky in the energy range from 20 MeV to above 300 GeV with its main instrument, the Large Area Telescope (LAT, [10]). The total γ-ray flux is originated by a diversity of astrophysical processes. Most of the photons in the GeV-range are induced by cosmic rays (CRs), charged particles moving at (ultra-)relativistic speeds, through hadronic interactions of CR nuclei with the interstellar medium (ISM) or inverse Compton scattering (IC) of electrons with background light [7, 18]. In addition, there is emission from a spatially constant diffuse background, which is commonly denoted as "extragalactic" background ([17], and references therein), and from sources that appear point-like.

The diffuse and point-like γ-ray fluxes appear superimposed to an observer. An observation through an instrument, like the *Fermi* LAT for example, additionally convolves the total flux with the instrument response functions (IRFs). The gathered data are, lastly, subject to noise, that is, Poissonian shot noise in the case of integer photon counts. To retrieve the physical photon flux from observations, we backward reconstruct flux contributions using Bayesian inference methods ([11, 15, 31, 35]). We deploy the D^3PO inference algorithm ([29]) derived within the framework of information field theory (IFT, [20, 21, 22]). It simultaneously provides non-parametric estimates for the diffuse and the point-like photon flux given a photon count map. D^3PO considers Poissonian shot noise, without Gaussian approximations, and takes the provided IRFs of the *Fermi* LAT fully into account. Furthermore, we can retrieve uncertainty information on the estimates. All this allows us to present a continuous reconstruction of the diffuse γ-ray sky up to around 300 GeV, as well as an estimate of the point-like contribution, from which we derive the first D^3PO *Fermi* catalog of γ-ray source candidates. By analyzing the spectral behavior of the diffuse component, it is possible to investigate the underlying processes, especially with regard to the CRs responsible for the emission.

We analyze the photon count data collected by the *Fermi* LAT within its 6.5 years of operation. We make use of the reprocessed Pass 7 available within the *Fermi* Science Tools to retrieve the data, as well as the corresponding instrument response functions and exposure of the *Fermi* LAT ([10, 1, 5]). We considered nine logarithmically spaced energy bands ranging from 0.6 to 307.2 GeV. For each band, we spatially binned all events classified as CLEAN in count maps, whereby we distinguished the front or back conversion of the photon within the LAT. Throughout this work, we discretize the sky using the HEALPIX scheme with $n_{side} = 128$, which corresponds to an angular resolution of approximately $0.46°$. For an extensive description of the algorithm, the adopted approach, and the results we refer to [30].

2. γ-ray sky

Figure 1 shows the maps of the γ-ray sky produced by D^3PO. To obtain a better view on the spectral characteristics of the γ-ray sky, we combine the maps at different energies with a pseudo-color scheme designed to mimic the human perception of optical light in the γ-ray range. Intensity indicates the (logarithmic) brightness of the flux, red corresponds to low-energy γ-rays around 1 GeV, and blue to γ-rays up to 300 GeV. Thanks to a suitably tuned color response, spectrally different regions can easily be identified by eye. At a first glance, we can recognize the bright bulge
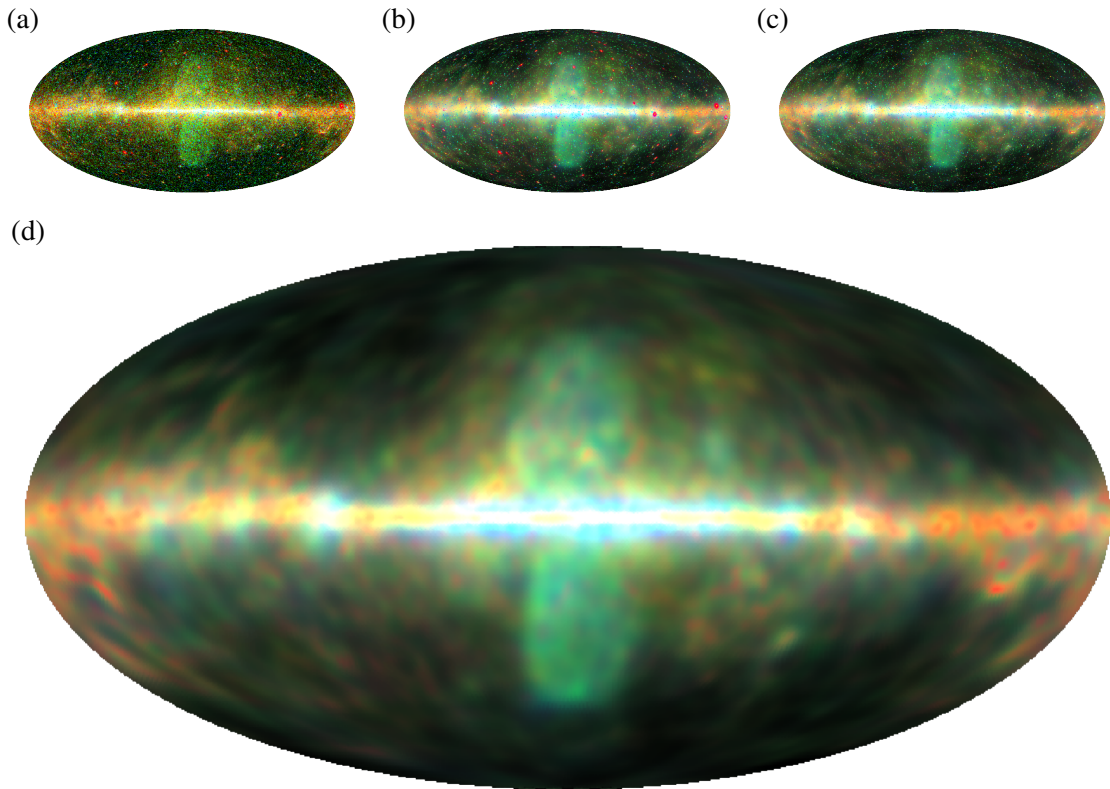
Figure 1: γ-ray sky in pseudocolor in a Mollweide projection. Panel (a) shows the 6.5 year data. Panels (b) and (c) show the reconstructed (total) photon flux that in (b) is reconvolved with the IRFs. Panel (d) shows the reconstructed diffuse photon flux. Credit: Selig et al. A&A, in press, DOI 10.1051/0004-6361/201425172, 2015, reproduced with permission ©ESO.

of the Milky Way, the *Fermi* bubbles as two slightly green-blue, somewhat round areas, and red to yellow cloud-like structures at low and intermediate latitudes, in particular around the Galactic anticenter.

The images illustrate the functionality of the D^3PO inference algorithm, showing the raw data and the denoised, deconvolved, and decomposed reconstruction. The denoising applies most strongly to the high-energy bands, which appear slightly green-blue, where the signal-to-noise ratios are lowest. The deconvolution effect is most evident for point-like contributions in lower energy bands, which appear slightly red, because of the increasing width of the point spread function (PSF) for these bands. Finally, the decomposition reveals the purely diffuse γ-ray sky.

This view reveals many interesting features beyond the Galactic disk and bulge. The most striking features recovered by our reconstruction are the *Giant Fermi Bubbles* first found by [33]. The bubbles extend up to $|b| \lesssim 50°$ in latitude and $|l| \lesssim 20°$ in longitude. They appear to emerge from the Galactic center, but their astrophysical origin is still under discussion ([33, 16, 13, 19, 34, 36, 8], and references therein). In agreement with previous studies, we find the bubbles to have relatively sharp edges and an overall homogeneous surface brightness; they appear slightly green-blue in Fig. 1. [36] reported an energy-dependent morphology of the southern bubble, which is, in
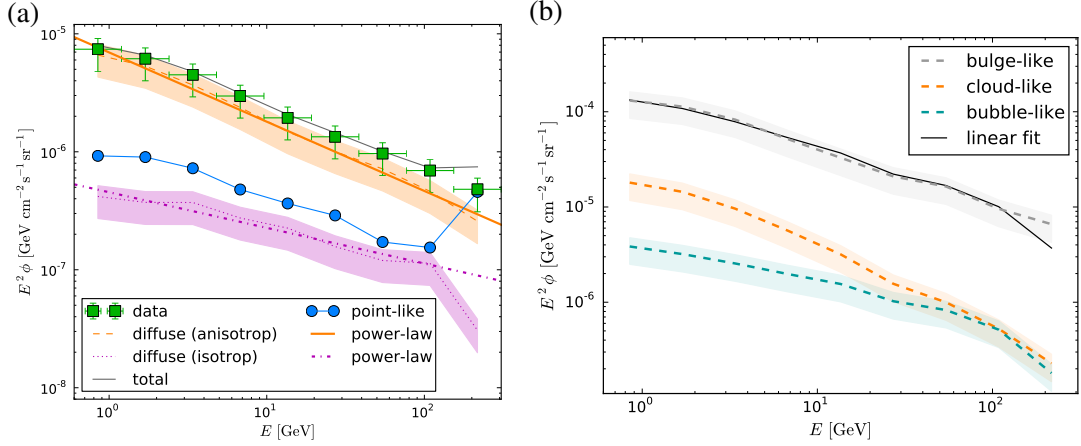
Figure 2: Panel (a): All sky energy spectra. Shown are the data (green squares) converted to flux units, and spectra from the reconstructed total (gray), anisotropic diffuse (dashed orange), isotropic diffuse (dotted magenta), and point-like photon flux (blue circles). Furthermore, power-law fits for the anisotropic (thick solid orange) and isotropic emission (thick dashed-dotted magenta) are shown. Panel (b) shows energy spectra from the regions of interest. In addition to the spectra retrieved from the different regions, a linear combination of the cloud-, and bubble-like is fit to the bulge-like component, cf. legend. Credit: Selig et al. A&A, in press, DOI 10.1051/0004-6361/201425172, 2015, reproduced with permission ©ESO.

particular, more extended to the Galactic south and west at high energies, confirmed by our results.

To obtain a more quantitative view on the different contributions to the γ-ray flux, we investigated photon flux energy spectra. Figure 2 (a) shows the measured and reconstructed energy spectra for the whole sky. The errors are dominated by systematics, by the uncertainty in the absolute energy scale and in the normalization of the effective area. The statistical uncertainties determined from the inference tend to track the signal-to-noise ratio.

We split the total energy spectrum into a diffuse and a point-like contribution, whereby we additionally distinguished between isotropic[1] and anisotropic diffuse components. Overall, the spectra from the reconstructed fluxes agree well with the data, except for the highest energy bin, where the point-like component seems to be strongly overestimated. There are two reasons for this. On the one hand, the signal-to-noise ratio is lowest, and on the other hand, the PSF is sharpest. Therefore, the distinction between point-like sources, noise peaks, and weak diffuse emission breaks down. For this reason, we excluded this highest energy band from further spectral analysis.

For the anisotropic component we find a spectral index $\gamma^{(s)} = 2.59 \pm 0.05$ that is slightly softer than the index of 2.44 ± 0.01 reported by [6], indicating a lack of flux at high energies, which can again be explained by the low signal-to-noise ratio in this regime. In low energy bands, the spectrum is dominated by the production and decay of π^0-mesons induced by CR protons, while IC emission becomes increasingly strong at the highest energies ([6, 5]).

The isotropic diffuse background also follows a featureless power law with a spectral index $\gamma_{\rm iso}^{(s)} = 2.30 \pm 0.06$, if we ignore the last energy band. The excess of isotropic emission around $\sim 3\,{\rm GeV}$ does not affect the uncertainties. [3] derived a spectral index of 2.41 ± 0.05 from one year *Fermi* LAT data in the energy range of 0.03–100 GeV. This indicates a slight spectral hardening

---

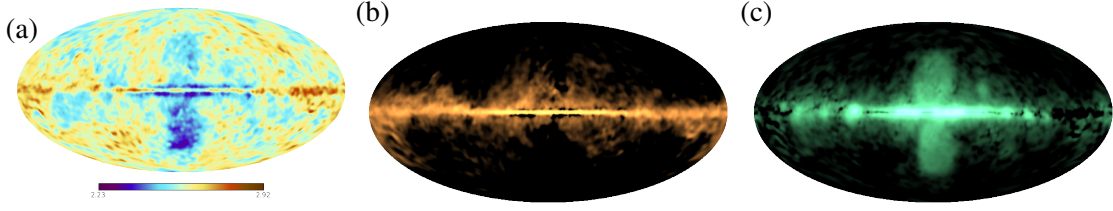[1]In this context, "isotropic" means spatially constant.

4

Figure 3: Panel (a): Spectral indices of featureless power-law fits, $\phi_{\mathrm{aniso}} \propto E^{-\gamma}$, at all positions in the sky using energy bands 1–8. Panel (b) shows the cloud-like and panel (c) the bubble-like diffuse component in pseudocolor in a Mollweide projection. Credit: Selig et al. A&A, in press, DOI 10.1051/0004-6361/201425172, 2015, reproduced with permission ©ESO.

of the isotropic background toward higher energies. In the same energy range, observations with the Energetic Gamma Ray Experiment Telescope (EGRET) yield a spectral index of 2.10 ± 0.03 that is considerably smaller ([32]). This discrepancy, which might be an instrumental problem, is not yet clarified. The recent analysis by [9], who investigated an energy range of 0.1–820 GeV, reported the isotropic γ-ray background to be consistent with a power law with exponential cutoff at 280 GeV that has a spectral index of 2.32 ± 0.02. This is consistent with our findings.

Since the D^{3}PO algorithm provides a continuous estimate of the diffuse photon flux, we performed a spectral analysis in individual pixels. Although the energy spectra vary with location, for simplicity, we assumed a general power-law behavior everywhere, but with varying spectral index. Figure 3 (a) shows the obtained spectral index map for the anisotropic γ-ray sky, centered on the average index of 2.6. The spatial smoothness of the spectral index map reflects that there are no discontinuities between neighboring pixels in the reconstructions. From this spectral index map it is apparent that the Galactic disk is spectrally softer than the all-sky average. The same holds for the extensive structures that trace interstellar gas. These regions are dominated by hadronic interactions releasing γ-ray photons, for example, π^0 production and decay (cf., e.g., [7]).

In the region overlapping with the *Giant Fermi Bubbles* we find overall similar spectra that are harder than the all-sky average, however. This agrees with the results of [8]. The strong hardening toward the high-latitude edge of the southern bubble arises because it is spatially more extented than at lower energies, cf. [36]. Additional local spots inside the bubble region are insignificant within the statistical and systematic uncertainties. Although the morphology and spectra of the bubbles can be explained with hadronic and leptonic CR processes, IC scenarios also enable reproducing the microwave haze observed with WMAP and *Planck* ([27, 37, 8]). Furthermore, the low target densities at higher Galactic latitudes render the hadronic scenario unsatisfactory.

3. Diffuse emission components

The pseudocolor scheme introduced in Sect. 2 already allows us to visually inspect the continuous reconstruction of the diffuse γ-ray sky. By eye, we can make out the Galactic bulge, the *Fermi* bubbles, and also cloudy structures around the Galactic anticenter.

To confirm this impression of the visualization, we retrieved energy spectra from three characteristic regions: bulge-like ($|l| < 40°, |b| < 1.5°$), cloud-like ($-150° < l < -120°, |b| < 3°$), and bubble-like (for which we selected the southern bubble up to latitudes $b < -27.5°$).

Figure 2b shows the energy spectra retrieved from the three regions. The cloud-like spectrum is rather soft ($\gamma^{(s)} \approx 2.6$) and features the tail of the pion bump. Note that the highest energy bin is unreliable due to the difficulty to discriminate between point sources and diffuse flux for the small number of photons there. As expected, the cloud-like spectrum is dominated by emission from π^0 decay, because the cloudy structures trace the gas content of the ISM that provides the target protons for π^0 production. The bubble-like spectrum is significantly harder ($\gamma^{(s)} \approx 2.4$), indicating the dominance of hard processes like IC emission. The bulge-like region exhibits a spectrum that, besides having a higher absolute scale, can be described as a linear combination of the former two spectra, cf. Fig. 2b.

As the bulge-like spectrum is found to be a linear combination of cloud- and bubble-like, we tried to decompose the whole diffuse sky into those two components. For this purpose, we fit the spectrum in individual pixels by the cloud- and bubble-like component.[2] The fit coefficients then indicate the strength of the cloud- or bubble-like contribution at all locations. Multiplying the fit coefficients with the respective spectra, we obtained a pseudocolor visualization of the cloud- or bubble-like emission components as shown in Fig. 3, panels (a) and (b).

In spite of the simplicity of this two-component model, the total diffuse emission and the sum of the two components agree well. The relative residuals are around 5–13%, except for the highest energy band, which was excluded from the fitting procedure, where the error is approximately 28%. Our findings demonstrate that the γ-ray sky in the energy range from 0.6 to 307.2 GeV can with high precision be described by cloud- and bubble-like emission components alone.

Since the bubble-like γ-ray emission is morphologically so distinct and different from the cloud-like component, we assume that the two components are dominated by different emission processes. The bubble-like spectrum is distinctly harder and less structured, therefore a leptonic emission process, in particular IC scattering, seems the more plausible origin for the bubble-like diffuse component. The CR populations producing these two γ-ray emission components do not need to be very different. It might be that we observe two different phases of the ISM. The cold and condensed phase carries most of the Galactic gas and has a sufficient nuclei target density to be predominately revealed through hadronic interactions with CR protons. Hence, the resulting γ-ray emission mostly traces the highly structured gas distribution. The hot, diluted, and voluminous phase tends to flow out of the Galactic disk. The γ-ray emission from within is dominated by IC upscattering of the Galactic photon field by CR electrons. As the photon field is relatively homogeneous, the morphology of the bubble-like component is probably shaped by the spatial distribution of the CRs. This simple two-component model of the diffuse γ-ray emission supports scenarios in which the *Fermi* bubbles are just outflows of the hot ISM ([37, 13, 19, 14, 12]).

3.1 Point sources

Another result of our analysis of the 6.5 year *Fermi* data is a reconstruction of the point-like contribution to the photon flux which consists of Galactic and extragalactic point sources.

Figure 4 shows an all-sky map of all point source candidates in the pseudocolor scheme introduced in Sect. 2. To nominate a candidate, we checked whether the point-like contribution

---

[2]When the fit suggests a negative coefficient for one component, the fitting procedure was repeated without this component. In this way, we ensured that the components were positive.
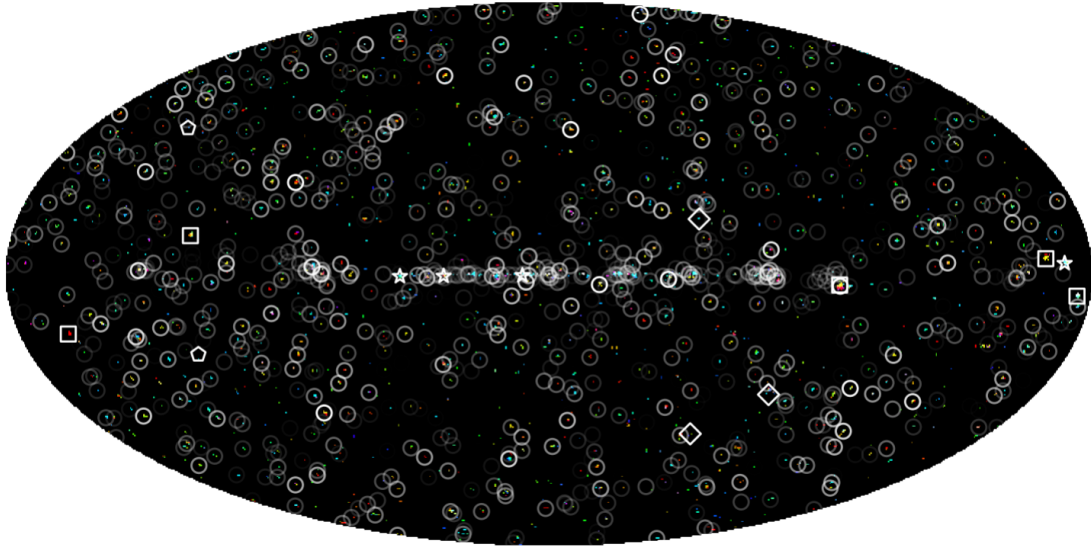
Figure 4: Point sources in the γ-ray sky in pseudocolor and in a Mollweide projection. Markers show point sources from the second *Fermi* LAT source catalog ([25]) for comparison; the gray scale indicates their average detection significance as listed in the catalog. Special markers show a selection of pulsars (squares), local SNRs (stars), and well-known galaxies (pentagons), as well as famous extragalactic objects (diamonds), cf. text. Credit: Selig et al. A&A, in press, DOI 10.1051/0004-6361/201425172, 2015, reproduced with permission ©ESO.

exceeded 2σ above the diffuse emission in at least two of the energy bands 1–8, which is a simple but conservative criterion taking the diffuse reconstruction uncertainty into account. We excluded the highest energy band from our search, since the point-like flux in this band seems to be contaminated. We refer to the compiled point source catalog as the first D^3PO *Fermi* (1DF) catalog of γ-ray source candidates. Qualitatively, the point-like flux found by D^3PO agrees with the second *Fermi* LAT source catalog as shown in Fig. 4.

We found 3,106 source candidates. For comparison, the one, two, and four year *Fermi* LAT source catalogs comprise 1,451, 1,873, and 3,034 sources, respectively ([2, 25, 4]). 1,381 (1,897) of our sources can be associated with known LAT sources from the second (third) catalog. The reason why we do not confirm all objects in the second (third) *Fermi* LAT source catalog is the conservative criterion we applied. This still leaves 1,253 (1,209) new source candidates to be confirmed by future work. In Fig. 5 we show a comparison of the second *Fermi* LAT source catalog and candidates from the reconstruction for which an association in the second *Fermi* LAT catalog has been found. Our catalog includes some galaxy clusters hosting diffuse radio sources (i.e. radio halos) which in our reconstruction appear point-like due to the pixelization. An analysis at higher resolution is necessary to localize and better understand the origin of this emission. If confirmed and not explained by embedded AGNs, this emission would be in favor of an hadronic origin for the relativistic electrons responsible of the observed diffuse radio emission.
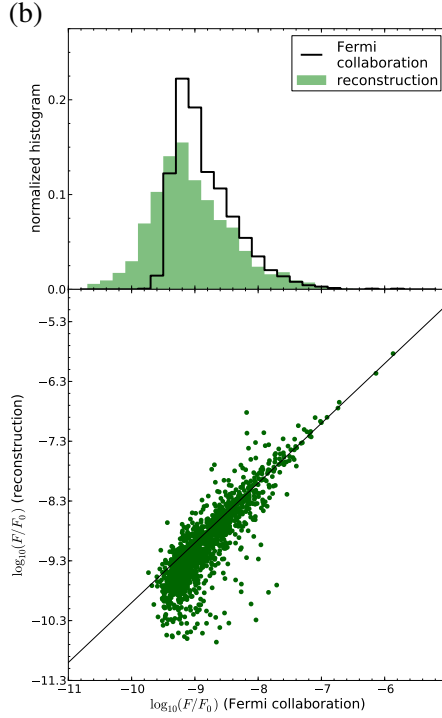
Figure 5: Comparison of the second *Fermi* LAT source catalog ([25]) and candidates from the reconstruction for which an association in the second *Fermi* LAT catalog has been found. The panels show the histogram and scatter plot of the logarithmic total fluxes $\log_{10}(F/F_0)$, where $F_0 = 1\,\mathrm{cm}^{-2}\,\mathrm{s}^{-1}$. The scatter plot contains a $1:1$ line (black solid) for comparison. Credit: Selig et al. A&A, in press, DOI 10.1051/0004-6361/201425172, 2015, reproduced with permission ©ESO.

4. Conclusions and summary

We analyzed the *Fermi* LAT 6.5 year photon data in the energy range from 0.6 to 307.2 GeV. We applied the inference algorithm D^{3}PO to effectively denoise, deconvolve, and decompose the data with Bayesian inference methods. In contrast to previous approaches by the *Fermi* collaboration and others, our non-parametric reconstruction does not rely on emission templates. We obtained estimates for the diffuse and point-like contributions to the γ-ray flux. The continuous reconstruction of the diffuse flux allowed us to present the first spectral index map of the diffuse γ-ray sky, as well as a pseudocolor composite visualizing the spectrally different regions.

Inspired by the pseudocolor visualization, we decomposed the diffuse γ-ray sky into a cloud-like and bubble-like emission component. The former, tracing the dense, cold ISM, is dominated by hadronic emission processes, while the latter, being morphologically and spectrally distinct, seems to be dominated by leptonic processes in hot, diluted parts of the ISM and outflows thereof. In particular, we confirm the existence of the *Giant Fermi Bubbles*, as well as their homogeneous morphology, sharp edges, and hard spectra. In particular, our findings indicate that their emission is likely due IC and support scenarios in which they are explained by hot outflows powered by strong activities in the Galactic center region ([37, 13, 19, 14, 12]).

The reconstruction of the point-like photon flux qualitatively confirms most of the sources from the second and third *Fermi* LAT source catalog. Quantitatively, we derived the first D^{3}PO

Fermi catalog of γ-ray source candidates that comprises 3,106 point sources including a few galaxy clusters hosting known radio halos.

Acknowledgments

References

[1] Abdo, A. A., Ackermann, M., Ajello, M., et al. 2009, *The on-orbit calibration of the Fermi Large Area Telescope*, Astroparticle Physics, 32, 193, (arXiv:0904.2226)

[2] Abdo, A. A., Ackermann, M., Ajello, M., et al. 2010, *Fermi Large Area Telescope First Source Catalog*, ApJS, 188, 405, (arXiv:1002.2280)

[3] Abdo, A. A., Ackermann, M., Ajello, M., et al. 2010b, *Spectrum of the Isotropic Diffuse Gamma-Ray Emission Derived from First-Year Fermi Large Area Telescope Data*, Physical Review Letters, 104, 101101, (arXiv:1002.3603)

[4] Acero, F., Ackermann, M., Ajello, M., et al. 2015, *Fermi Large Area Telescope Third Source Catalog*, ApJS, 218, 23, (arXiv:1501.02003)

[5] Ackermann, M., Ajello, M., Albert, A., et al. 2012, *The Fermi Large Area Telescope on Orbit: Event Classification, Instrument Response Functions, and Calibration*,ApJS, 203, 4, (arXiv:206.1896)

[6] Ackermann, M., Ajello, M., Albert, A., et al. 2012b, *Fermi LAT search for dark matter in gamma-ray lines and the inclusive photon spectrum*, Physical Review D, 86, 022002, arXiv:1205.2739)

[7] Ackermann, M., Ajello, M., Atwood, W. B., et al. 2012d, *Fermi-LAT Observations of the Diffuse Gamma-Ray Emission: Implications for Cosmic Rays and the Interstellar Medium*, ApJ, 750, 3, (arXiv:1202.4039)

[8] Ackermann, M., Albert, A., Atwood, W. B., & Fermi LAT Collaboration, 2014, *The Spectrum and Morphology of the Fermi Bubbles*, ApJ, 793, 64, (arXiv:1407.7905)

[9] Ackermann, M., Ajello, M., Albert, A., et al., 2015, *The spectrum of isotropic diffuse gamma-ray emission between 100 MeV and 820 GeV*, ApJ, 799, 86, (arXiv:1410.3696)

[10] Atwood, W. B., Abdo, A. A., Ackermann, M., et al. 2009, *The Large Area Telescope on the Fermi Gamma-Ray Space Telescope Mission*, ApJ, 697, 1071, (arXiv:0902.1089)

[11] Bayes, T. 1763, *An Essay towards Solving a Problem in the Doctrine of Chances*, Philosophical Transactions of the Royal Society 35, 370 – 418

[12] Carretti, E., Crocker, R. M., Staveley-Smith, L., et al., 2013, *Giant magnetized outflows from the centre of the Milky Way*, Nature, 493, 66, (arXiv:1301.0512)

[13] Cheng, K.-S., Chernyshov, D. O., Dogiel, V. A., Ko, C.-M., & Ip, W.-H., 2011, *Origin of the Fermi Bubble*, ApJl, 731, L17, (arXiv:1103.1002)

[14] Chernyshov, D., 2011, *Particle acceleration and the origin of gamma-ray emission from Fermi Bubbles*, International Cosmic Ray Conference, 7, 11, (arXiv:1109.2619)

[15] Cox, R. T. 1946, *Probability, Frequency and Reasonable Expectation*, American Journal of Physics 14, 1

[16] Crocker, R. M., & Aharonian, F., 2011, *Fermi Bubbles: Giant, Multibillion-Year-Old Reservoirs of Galactic Center Cosmic Rays*, Physical Review Letters, 106, 101102

[17] Dermer, C. D. 2007, *The Extragalactic γ Ray Background*, The First GLAST Symposium, 921, 122, (arXiv:0704.2888)

[18] Dermer, C. D., Strong, A. W., Orlando, E., Tibaldo, L., & for the Fermi Collaboration 2013, *Determining the Spectrum of Cosmic Rays in Interstellar Space from the Diffuse Galactic Gamma-Ray Emissivity*, arXiv:1307.0497

[19] Dogiel, V. A., Chernyshov, D. O., Cheng, K., Wang, Y., Ko, C., & Ip, W., 2011, *Fermi Bubbles as a Result of Star Capture in the Galactic Center*, arXiv:1109.6087

[20] Enßlin, T. A., Frommert, M., & Kitaura, F. S. 2009, *Information field theory for cosmological perturbation reconstruction and nonlinear signal analysis*, Physical Review D, 80, 105005, (arXiv:0806.3474)

[21] Enßlin, T. 2013, *Information field theory*, American Institute of Physics Conference Series, 1553, 184, (arXiv:1301.2556)

[22] Enßlin, T. 2014, *Astrophysical data analysis with information field theory*, in American Institute of Physics Conference Series, arXiv:1405.7701

[23] Górski, K. M., Hivon, E., Banday, A. J., et al. 2005, *HEALPix: A Framework for High-Resolution Discretization and Fast Analysis of Data Distributed on the Sphere*, ApJ, 622, 759, (arXiv:astro-ph/0409513)

[24] Hunter, J. D., 2007, *Matplotlib: A 2D graphics environment*, Computing In Science & Engineering, IEEE COMPUTER SOC, 9, 3

[25] Nolan, P. L., Abdo, A. A., Ackermann, M., et al. 2012, *Fermi Large Area Telescope Second Source Catalog*, ApJS, 199, 31, (arXiv:1108.1435)

[26] Oliphant, T., 2006, *A Guide to NumPy*, Trelgol Publishing

[27] Planck Collaboration, Ade, P. A. R., Aghanim, N., et al., 2013, *Planck intermediate results. IX. Detection of the Galactic haze with Planck*, A&A, 554, A139, (arXiv:1208.5483)

[28] Selig, M., Bell, M. R., Junklewitz, H., et al. 2013, *NIFTY - Numerical Information Field Theory - a versatile Python library for signal inference*, A&A, 554, A26, (arXiv:1301.4499)

[29] Selig, M., & Enßlin, T. A. 2015, *Denoising, Deconvolving, and Decomposing Photon Observations*, A&A, 574, A74, (arXiv:1311.1888)

[30] Selig, M., Vacca, V., Oppermann, N., & Enßlin, T. A. 2014, arXiv:1410.4562

[31] Shannon, C. E. 1948, *A mathematical theory of communication*, Bell System Technical Journal 27, 379 – 423

[32] Sreekumar, P., Bertsch, D. L., Dingus, B. L., et al., 1998, *EGRET Observations of the Extragalactic Gamma-Ray Emission*, ApJ, 494, 523

[33] Su, M., Slatyer, T. R., & Finkbeiner, D. P. 2010, *Giant Gamma-ray Bubbles from Fermi-LAT: Active Galactic Nucleus Activity or Bipolar Galactic Wind?*, ApJ, 724, 1044, (arXiv:1005.5480)

[34] Su, M., & Finkbeiner, D. P., 2012, *Evidence for Gamma-Ray Jets in the Milky Way*, ApJ 753, 61, (arXiv:1205.5852)

[35] Wiener, N. 1949, *Extrapolation, Interpolation and Smoothing of Stationary Time Series, with Engineering Applications*, Technology Press and Wiley, New York, note: Originally issued in Feb 1942 as a classified Nat. Defense Res. Council Rep.

[36] Yang, R.-z., Aharonian, F., & Crocker, R., 2014, *The Fermi bubbles revisited*, A&A, 567, A19, (arXiv:1402.0403)

[37] Yang, H.-Y. K., Ruszkowski, M., & Zweibel, E., 2013, *The Fermi bubbles: gamma-ray, microwave and polarization signatures of leptonic AGN jets*, MNRAS, 436, 2734, (arXiv:1402.0403)

PoS(ICRC2015)768